Transdermal diffusion, spatial distribution and physical state of a potential anticancer drug in mouse skin as studied by diffusion and spectroscopic techniques

Quoc-Chon Le[a,b,c], Thierry Lefèvre[a], René C.- Gaudreault[b,d], Gaétan Laroche[b,c], and Michèle Auger[a]

[a]*Département de chimie, PROTEO, CERMA, CQMF, Université Laval, Québec, Québec, Canada, G1V 0A6*
[b]*Laboratoire d'ingénierie de surface, Centre de recherche du CHU de Québec, Hôpital St-François d'Assise, 10 rue de l'Espinay, Québec, Québec, Canada, G1L 3L5*
[c]*Département de génie des mines, métallurgie et matériaux, CERMA, Université Laval, Québec, Québec, Canada, G1V 0A6*
[d]*Département de médecine moléculaire, Université Laval, Québec, Québec, Canada, G1V 0A6*

ABSTRACT

Understanding the efficiency of a transdermal medical drug requires the characterization of its diffusion process, including its diffusion rate, pathways and physical state. The aim of this work is to develop a strategy to achieve this goal. FTIR spectroscopic imaging in conjunction with a Franz cell and HPLC measurements were used to examine the transdermal penetration of deuterated tert-butyl phenylchloroethylurea (tBCEU), a molecule with a potential anticancer action. tBCEU has been solubilized in an expedient solvent mixture and its diffusion in hairless mouse skin has been studied. The results indicate that tBCEU diffuses across the skin for more than 10 hours with a rate comparable to selegiline, an officially-approved transdermal drug. IR image analyses reveal that after 10 hours, tBCEU penetrates skin and that its spatial distribution does not correlate with neither the distribution of lipids nor proteins. tBCEU accumulates in cluster domains but overall low concentrations are found in skin. FTIR spectroscopic imaging additionally reveals that tBCEU is in a crystalline form. The results suggest that tBCEU is conveyed through the skin without preferential pathway. FTIR spectroscopic imaging and transdermal diffusion measurements appear as complementary techniques to investigate drug diffusion in skin.

KEYWORDS
Infrared microspectroscopy, Tert-butyl phenylchloroethylurea, Diffusion pathway, Diffusion kinetics, Drug physical state, Franz cell, HPLC

CITATION
Le, Q. C., Lefèvre, T., C-Gaudreault, R., Laroche, G., & Auger, M. (2018). Transdermal diffusion, spatial distribution and physical state of a potential anticancer drug in mouse skin as studied by diffusion and spectroscopic techniques. Biomedical Spectroscopy and Imaging, 7(1-2), 47-61.

This is the author's version of the original manuscript. The final publication is available at IOS Press Link Online via DOI 10.3233/BSI-180179

1 INTRODUCTION

Drugs can enter the body following several administration routes, notably enteral (e.g., oral and rectal), parenteral (e.g., intravenous and intramuscular) and topical (e.g., inhalation and

epicutaneous). The latter is a form of transdermal drug delivery (TDD), which has been proven a good method for drug administration [1]. TDD avoids the hepatic first-pass metabolism, improves bioavailability, increases the compliance of patients and avoids accidents during injection [2-5]. However, TDD strategy encounters the effective hindrance of the stratum corneum (SC), the outermost layer of skin and the principal barrier against transdermal diffusion. Consequently, only a few commercial drugs have been delivered using the TDD method [2,4]. Generally, drug molecules must satisfy some criteria in order to efficiently diffuse through the skin. Among them are molecular weight (< 400-500 Da) and lipophilicity (log P varies between 2 and 3, P being the partition coefficient between octanol and water) [4,6].

Phenylchloroethylurea derivatives (CEUs) are promising alkylating anticancer drugs, alkylating notably beta tubulin and prohibitin-1 [7-11]. CEUs were initially designed from the pharmacophoric moiety of aliphatic 2-chloroethylnitrosoureas such as carmustine and the biofunctional moiety of aromatic nitrogen mustards such as chlorambucil. CEUs subsets substituted with branched alkyl moieties, exemplified by tert-butyl CEU (tBCEU) (Fig. 1a), were shown to exhibit the highest cytotoxicity among the CEU family [8,12]. tBCEU has a molecular weight of 254.5 $g.mol^{-1}$ and a log P value of 3.2, which makes it a good candidate for transdermal diffusion [13]. A previous study indicates that the presence of this molecule in phospholipid bilayers decreased the gel-to-fluid phase transition temperature of lipids [13], suggesting that it may penetrate skin through intercellular lipid layers and enter the systemic circulation. This hypothesis remains however to be validated with real skin.

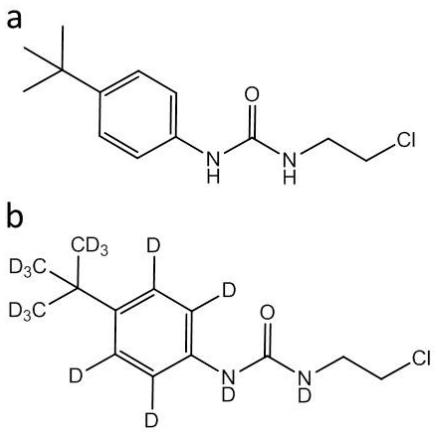

Figure 1. Molecular structure of (a) tBCEU and (b) tBCEU-d_{15}.

To adequately understand the efficiency of a transdermal medical drug, it is necessary to characterize its bioactivity (therapeutic and side effects) and its behavior within skin. In the latter case, it is required to determine the kinetics and pathways of diffusion as well as the drug conformation or physical state in skin. Such a characterization requires the use of complementary techniques. Taking tBCEU as an archetypal drug and mouse skin as a model of dermal barrier, we have used a Franz cell, HPLC and Fourier-transform infrared (FTIR) spectroscopic imaging to obtain a global view of the transdermal diffusion process. First, to validate the occurrence of diffusion through the skin, a Franz cell was used [14]. We associated this widespread technique with HPLC to measure the amount of drug that passes through the skin and to estimate the diffusion kinetics. Then, the spatial distribution of the drug inside skin layers was inferred from skin sections using FTIR spectroscopic imaging.

Although vibrational spectroscopy is still not widespread in dermatological studies, it has been proven useful to characterize skin [15,16] and skin substitutes [17,18] and to investigate the presence of exogenous molecules in skin without the use of markers [19,20]. Barry and coworkers

initiated the use of FTIR spectroscopy to study the stratum corneum [21]. Garidel and collaborators then pioneered the depth profile and lateral characterization of pig skin sections by using FTIR spectroscopic imaging [22]. The authors monitored the spatial distribution of proteins and lipids in skin according to their characteristic vibrational band intensities. Mendelsohn and coauthors published the first FTIR images of transdermal percutaneous absorption [23]. They found that DMSO and propylene glycol (PG) deeply penetrated pig skin and suggested that DMSO and PG distributions correlated with that of proteins.

In the present work, FTIR spectroscopic imaging was used to obtain snapshots of the spatial distribution of the drug in skin slices while allowing the characterization of its physical state. To avoid the overlap between the spectral contribution of tBCEU and those of the skin matrix, and thus to be able to spectroscopically probe the drug, tBCEU has been perdeuterated (tBCEU-d_{15}). The results presented show that a combination of analytical techniques, i.e. a Franz cell, HPLC and FTIR spectroscopic imaging has the potential to provide complementary information about the transdermal diffusion of drug across skin, including its diffusion kinetics, spatial distribution and physical state. The approach applied in this work may fruitfully be generalized to other bioactive molecules.

2 METHODS

2.1 Materials

The reactants for the synthesis of tBCEU-d_{15} were commercially available products: 4-tert-butylaniline-d_{15} (99.2 atom % D from C/D/N Isotopes Inc., Pointe-Claire, Québec, Canada), 2-chloroethylisocyanate (Sigma-Aldrich, Oakville, Ontario, Canada). Other analytical grade chemicals, ethanol, oleic acid and propylene glycol, were purchased from Sigma-Aldrich.

Nine-week old and hairless mice were sacrificed according to our institutional animal care committee procedures. The skin on the back of mice was surgically removed and kept in a DMEM (Dulbecco's Modified Eagle Medium) culture media at 4°C overnight, and were subsequently cut into pieces of 1.5 cm^2, and kept at -20 °C for experiment within 1 month. For Franz cell experiments, the subcutaneous fat was removed from the skin by scalpel.

2.2 Synthesis of tBCEU-d_{15}

Deuterated tBCEU (tBCEU-d_{15}, Fig. 1b) was synthesized according to a previously published protocol [24]. tBCEU-d_{15} was recovered by filtration and purified by recrystallizing in cold ethanol (1-4°C). The purity of tBCEU-d15 powder was higher than 98 %, verified by solution 1H NMR and HPLC.

2.3 Diffusion experiments with a Franz cell

A home-made horizontal Franz cell was used for diffusion experiment. It was composed of a donor and an acceptor chamber separated by the skin specimen barrier. tBCEU could diffuse through the membrane from the donor to the acceptor chamber (each having a volume of 800 µL). The orifice diameter of the Franz cell was 0.8 cm, which is equivalent to an effective diffusion area of 0.5 cm^2. Aliquots (30 µl) were sampled from the acceptor chamber at different time periods for analysis. For each aliquot collected, the same volume of PBS and DMSO was immediately added to keep the acceptor solution volume unchanged.

The donor chamber was filled with a tBCEU-d_{15} solution. To this end, tBCEU-d15 was dissolved at a concentration of 3.5 % w/w in a 2:1:1 volume ratio mixture of ethanol, propylene glycol and oleic acid. These solvents have been traditionally used as chemical enhancer for transdermal absorption [25,26]. Mixture of 70 % ethanol and 30 % of propylene glycol was used for trans-retinol transdermal

delivery study [27]. Propylene glycol is suitable for poor-soluble material such as tBCEU. Oleic acid, with its long-chain hydrocarbon, facilitates the solubility of tBCEU. The acceptor chamber was filled with a mixture of phosphate buffered-saline (PBS) pH 7.4 containing 2 % w/w of DMSO. The presence of DMSO facilitated the solubilization of tBCEU-d_{15} in the PBS solution.

The experiments were carried out in an oven at 32 °C with a constant humidity guaranteed by a wide-mouth water bath. After 10 hours, the experiment was stopped, the skin pieces taken out and rinsed twice with about 5 mL ethanol and 10 mL distilled water. This skin was then refrozen at -20 °C and microtomed for spectroscopic analysis (see below).

2.4 HPLC assay for diffusion studies

The aliquots collected from the receptor chamber of Franz cell were analyzed by HPLC (1200 Infinity series - Agilent Technologies, Santa Clara, CA, USA). The chromatograph was equipped with a UV detector (190-400 nm). A Vydac protein-peptide C18 column was used for analysis with a flow rate of the mobile phase (40 % H_2O and 60 % methanol) of 1 mL/min. Aliquots taken from the acceptor chamber (30 µL) were diluted with 270 µL of ethanol and were transferred into the HPLC, injected and analyzed. tBCEU-d_{15} yielded a single peak at 239 nm after a retention time of about 7.5 min. The correlation coefficient for the regression of the calibration curve is 0.993.

2.5 FTIR spectroscopic imaging

The skin pieces were embedded in Optimum Cutting Temperature (OCT) gel and sectioned vertically with a microtome at -20 °C into 12-µm thick slices. Typical skin surface and microtomed slices are shown in Fig. 2a and Fig. 2b, respectively. Skin slices were then placed on CaF_2 windows (thickness of 4 mm) for FTIR spectroscopic imaging analysis.

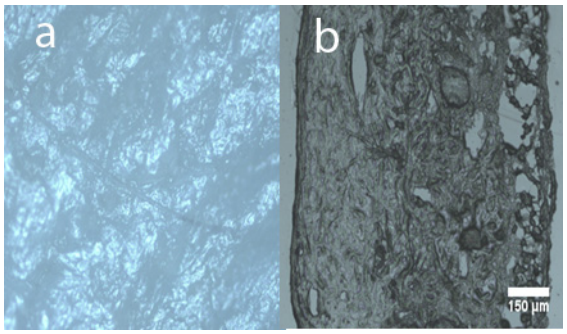

Figure 2. Optical images of a typical mouse skin specimen. Surface texture (a) and vertical section of 12 µm (b) after the diffusion experiment. The thickness of the skin is in the range of 700-1000 µm.

FTIR spectroscopic images were recorded with an Agilent 620 IR microscope, which is equipped with a liquid nitrogen-cooled 32×32 focal plane array (FPA) detector and a motorized stage. The FPA detector has pixel resolution of 5.5 μm^2 in transmission and reflection mode. The microscope is equipped with 4× and 15× objectives and attached to an Agilent 660 spectrometer.

IR images were recorded in transmission mode at a resolution of 4 cm^{-1} using 128 scans. A background image was taken from CaF_2 windows. Since skin sections are very thin and contain a very small amount of water after a few hours, especially during IR imaging measurements (each recording takes at least 20 minutes), the amount of remaining H_2O in the samples was very small so that H_2O subtraction was not necessary. At least three images, at different positions, were recorded on one slice of skin. The experiments were carried out on 10 slices cut from two pieces of skin (from two diffusion experiments) and the results were analyzed with Resolution Pro software (Varian) and GRAMS/AI (Thermo Fisher Scientific, Waltham, MA USA).

The linear correlation coefficients [28] between pair of absorbance were calculated according to the mathematical approach developed by Rodgers and Nicewander [29]. A correlation coefficient value of 1 implies that the variables have absolute correlation. Conversely, a value of zero indicates that the variables do not correlate with each other. The absorbance of the amide I, amide II, $\nu s(CH_2)$, $\nu as(CH_2)$ and CD_3 bands were taken from 50 different pixels, where the low absorbance of tBCEU-d15 could be measured with accuracy. The pixels were chosen from different slices of skin, 10 pixels from each slice and the corresponding correlation coefficients were calculated. The final value of the coefficients is the average of five values from five skin slices.

3 RESULTS

3.1 Franz cell combined with HPLC

Fig. 3 shows the amount of diffused tBCEU-d_{15} in the acceptor solution measured by HPLC as a function of time. The results indicate that tBCEU-d_{15} was detected in the acceptor solution after one hour of diffusion. The amount of diffused tBCEU-d_{15} increases linearly with time. After 10 hours of experiment, the amount of diffused tBCEU-d_{15} has not reached equilibrium, i.e. still increases. The concentration of tBCEU-d_{15} in the receptor solution after 10 hours of diffusion is 500 µmol/L, which shows that 0.5 % of tBCEU-d_{15} in the donor solution has passed through full-thickness mouse skin. Diffusion occurs with a rate of 0.075 µmol/cm^2/h or 20 µg/cm^2/h.

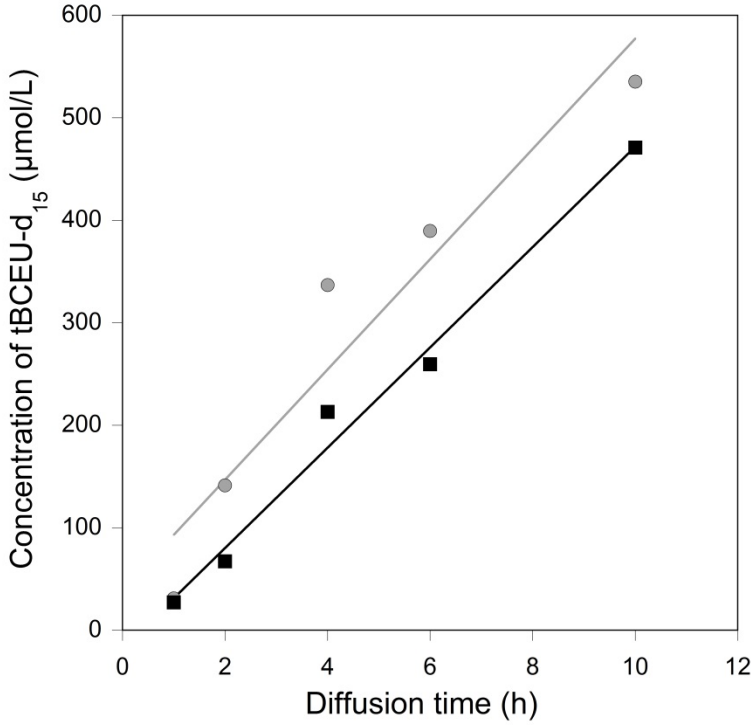

Figure 3. Variation of tBCEU-d_{15} concentration in the receptor solutions as a function of diffusion time through mouse skin. Circles and squares represent duplicated experiment data points. Full lines represent regression calculation of the experimental data points.

3.2 FTIR spectroscopic images

Representative IR spectra of mouse skin in the absence and presence of tBCEU-d_{15} are shown in Fig. 4. Positions of the main absorption bands and their assignment are shown. The predominant

spectral features originating from the skin matrix are due to proteins and lipids. The most intense bands characterizing proteins are the amide A vibration (N-H stretching) near 3300 cm^{-1}, the amide I vibration (~ 80 % C=O stretching) near 1655 cm^{-1}, the amide II vibration (~ 60 % N-H in-plane bending and 40 % C-N stretching) near 1550 cm^{-1} and the amide III vibration (N-H bending and C-N stretching) near 1240 cm^{-1} [30,31]. Those of lipids are the symmetric ($\nu_s(CH_2)$) and antisymmetric ($\nu_{as}(CH_2)$) stretching modes of CH_2 groups in the 2750-3050-cm^{-1} region, the lipid ester stretching ($\nu(C=O)$) mode near 1745 cm^{-1} and the deformation mode of the CH_2 groups ($\delta(CH_2)$) near 1455 cm^{-1}.

As can be seen, skin components can display numerous vibrational bands in various regions of the infrared spectrum, especially in the C-H stretching region. To easily distinguish the drug from skin, tBCEU was deuterated so that tBCEU could be probed via its unique C-D stretching vibrational bands which arise in a spectral region free from spectral contributions of the skin matrix. The presence of tBCEU-d15 is revealed by a small band centered near 2216 cm-1, assigned to the antisymmetric CD_3 stretching ($\nu_{as}(CD_3)$) (Fig. 4) [32]. Other bands due to tBCEU-d_{15} are the N-D stretching band [33] centered at 2500 cm^{-1} and the C-D stretching band of aromatic ring in the 2240-2310 cm^{-1} range [34]. Nevertheless, the latter bands are too weak to be clearly distinguished in the skin matrix.

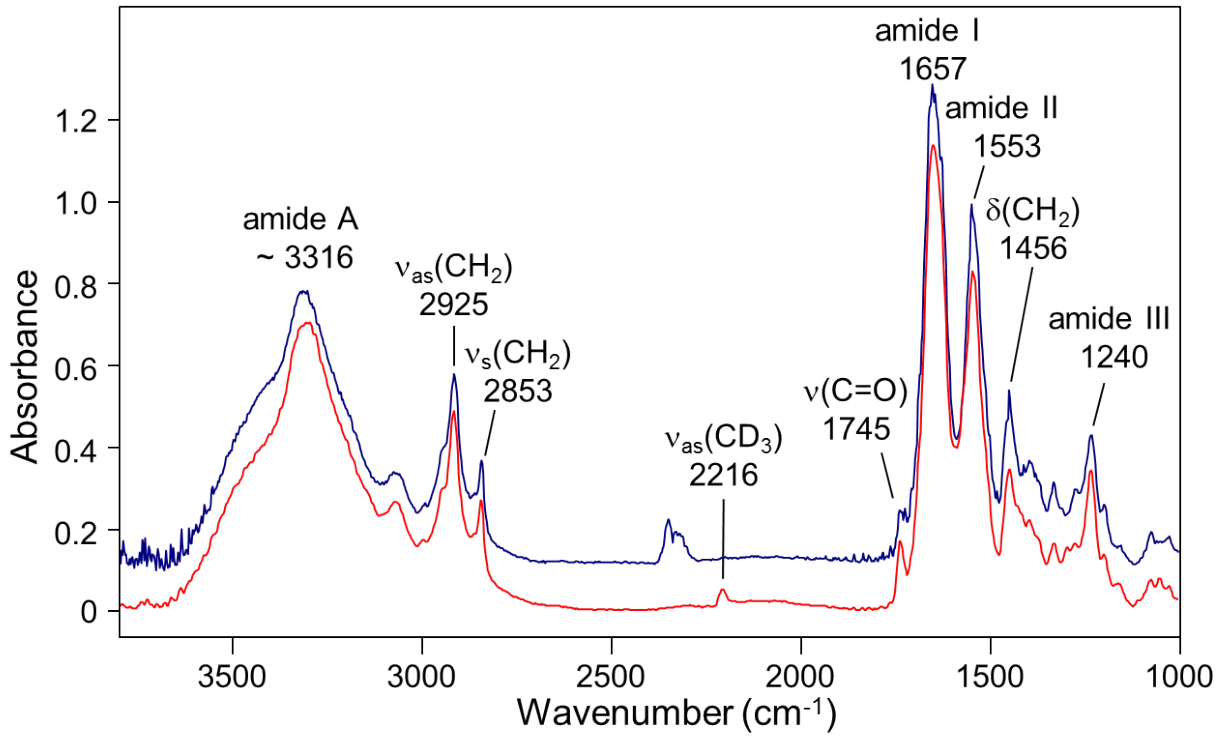

Figure 4. Typical IR spectra of mouse skin in the absence (blue spectrum) and presence (red spectrum) of tBCEU-d_{15}. Spectra are normalized with respect to the peak maxima and are shifted vertically for clarity reasons.

Fig. 5a displays an optical image of a typical perpendicular skin slice and the corresponding spatial distribution of tBCEU-d15 is shown in Fig. 5b as probed by the peak area (integrated intensity) at 2216 cm^{-1}. The image indicates that tBCEU-d15 is mainly concentrated at different locations in skin layers. The distribution of lipids (Fig. 5c) and proteins (Fig. 5d), measured according to the intensity of the $\nu_s(CH_2)$ and amide I bands, respectively, are also shown.

Fig. 5 reveals that the spatial distribution of tBCEU-d_{15} does not significantly overlap neither with that of lipids nor with that of proteins. Alternately, tBCEU-d_{15} seems to be distributed relatively homogeneously throughout the skin at low concentration, but part of it strongly accumulates in the form of clusters in some regions of the skin (green/yellow areas). As judged from the overall low intensity of the tBCEU signal (light blue background), the drug seems to be distributed at low concentration throughout mouse skin.

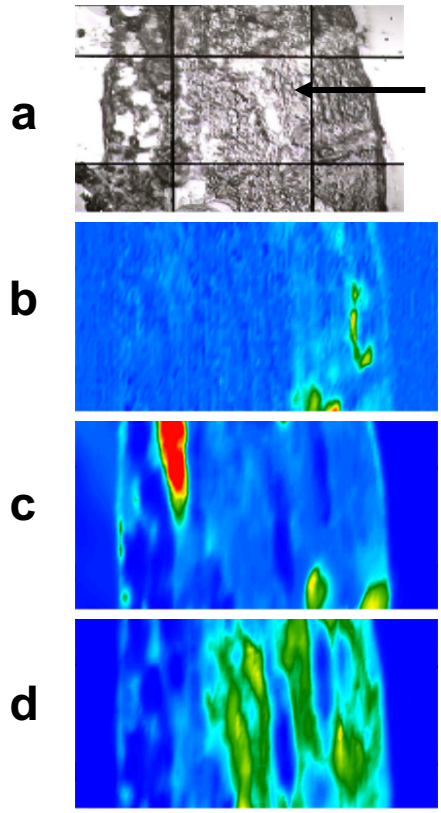

Figure 5. Optical and IR images of a mouse skin section. (a) Visible image (15×) showing the location where the infrared image was recorded. The black arrow indicates the diffusion direction of tBCEU-d15. Mouse skin IR image according to band intensity from (b) tBCEU-d_{15} ($v_{as}(CD_3)$), (c) lipids ($v_s(CH_2)$) and (d) proteins (amide I). Maps (e) and (f) represent the map ratios (c)/(d) and (d/c), respectively. The red color corresponds to the highest intensity and the blue indicates the lowest.

3.3 Correlations between IR intensities

To obtain more details regarding the relation between the spatial distribution of tBCEU with those of lipids and proteins, correlation coefficients measured between band intensities of tBCEU-d_{15}, proteins (amide I and amide II) and lipids ($v_{as}(CH_2)$ and $v_s(CH_2)$) have been calculated (Table I). We assumed a priori that the distribution of tBCEU has some kind of correlation with that of proteins or/and lipids. If this assumption is correct, we should find strong correlation at areas where tBCEU is concentrated.

As can be seen, the spatial distribution correlation coefficient between the amide I and amide II peak absorbance is 0.8, indicating a close relationship between these two bands. Such a correlation is of course expected since both bands are due to protein amide bonds. Similarly, the correlation coefficient between the $v_{as}(CH_2)$ and $v_s(CH_2)$ bands is 0.75, which is also an anticipated result since these bands mainly originate from lipid chains. By contrast, the correlation coefficient value between the absorbance of tBCEU-d_{15} (vas(CD_3)) and lipids is very small (0.048 and - 0.151, with the $v_{as}(CH_2)$

and $\nu_s(CH_2)$ mode, respectively), while the value between the absorbance of tBCEU-d15 and proteins reaches intermediate values, i.e. - 0.361 (amide II) and - 0.416 (amide I).

These values show that tBCEU-d_{15} spatial distribution is not correlated with that of lipids but that it may be weakly associated with that of protein-rich components. In the latter case, the negative value of the coefficients would indicate that when the abundance of proteins increases, that of tBCEU-d_{15} decreases, and vice versa. This result would thus suggest that tBCEU diffuses more efficiently in areas where the protein concentration is low. This may appear paradoxical. In fact, this result may be interpreted straightforwardly such as the drug has certain affinity for regions poor in proteins. However, the result may alternately, and indirectly, indicate that these regions are actually rich in (an)other undetected constituent(s) (not lipids), thus suggesting that tBCEU would have an affinity for this(these) putative component(s). Finally, due to the relatively low values of the correlation, it is possible that the tBCEU distribution is not correlated with that of proteins (nor lipids).

3.4 Using band shapes to determine the physical state of tBCEU

It has been found in the course of the experiments that tBCEU exhibits a propensity to crystallize (its fusion temperature is approximately 125 °C). For example, a solution of tBCEU in DMSO deposited on skin formed crystals after three hours, as seen in Fig. 6a. These crystals could easily be washed with water and ethanol (Fig. 6b).

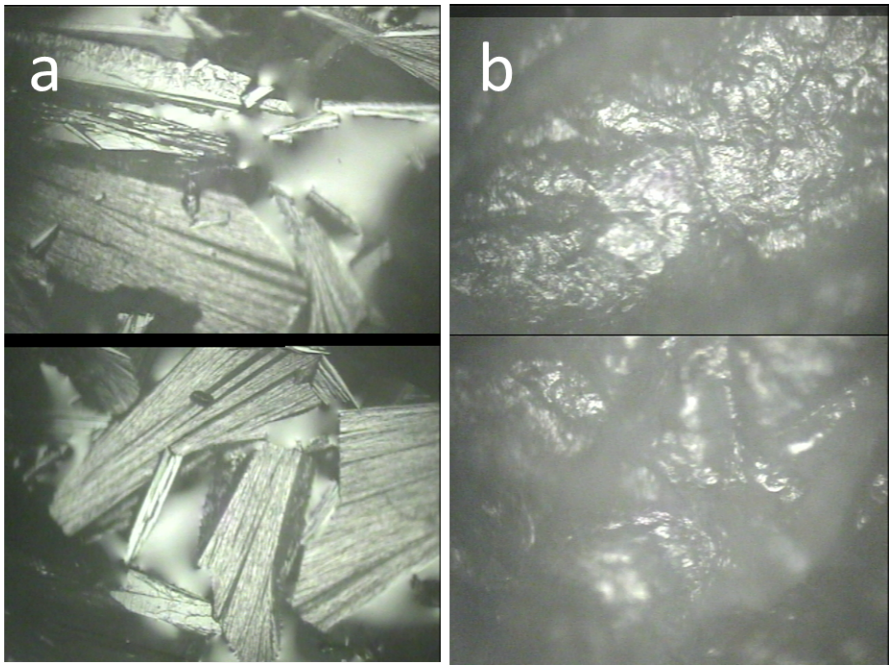

Figure 6. (a) Crystals of tBCEU-d_{15} on the surface of the skin after deposition (and solvent evaporation) of a tBCEU-d15 propylene glycol-ethanol solution. (b) Surface of the skin after washing with H2O and ethanol.

In the above diffusion experiments, tBCEU did not crystallize at the skin surface. However, it may be wondered on the physical state of the molecule within the skin. Fig. 7 shows that the $\nu_{as}(CD_3)$ band of tBCEU in solution (i.e., in the excipient solvent mixture) is symmetrical with a maximum at 2216 cm^{-1}. In the crystalline (solid) form, however, the $\nu_{as}(CD_3)$ band is constituted by a doublet at 2213 and 2220 cm^{-1}. Such an influence of the physical state on the $\nu_{as}(CD_3)$ band splitting is consistent with data regarding CD_3OH [35]. Indeed, the liquid form of CD_3OH gives rise to one component near 2232 cm^{-1} whereas the solid form (either amorphous or crystalline form) is

characterized by two components at 2213 and 2235 cm^{-1}. Thus, this spectral feature can be used to probe the physical state of tBCEU. In the skin matrix, the $\nu_{as}(CD_3)$ band of tBCEU is systematically composed of two components indicating that this drug is in a crystalline or solid state. The difference in the intensity ratio between in situ and crystalline tBCEU may reflect different crystalline forms. Alternately, the two peaks may represent two different polymorphs that would differ in proportion.

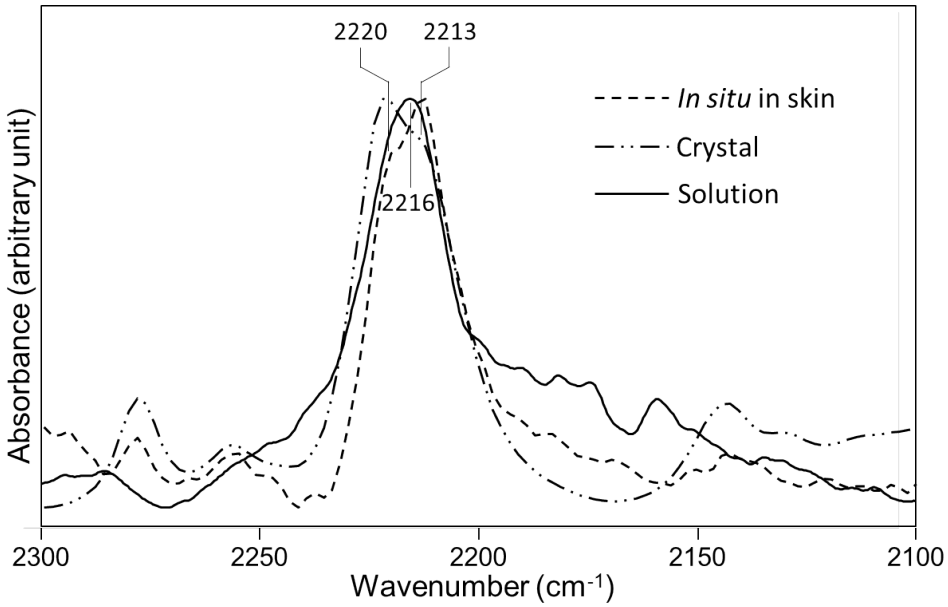

Figure 7. Spectra of tBCEU-d15 in different physical states: in ethanol-propylene-oleic acid solution with volume ratio of 2:1:1 (full line), in crystal form (dashed-dotted line) and in situ in mouse skin (dashed line). Spectra are normalized with respect to the peak maxima.

4 DISCUSSION

4.1 The amount of tBCEU available for a potential cancer treatment

In order to be used in transdermal delivery, drug molecules must overcome two difficulties: their pharmacological potency and skin permeability. Since over 30 years, there have been less than 20 compounds approved for commercial market in Europe and USA [4]. Among the approved drugs, nicotine has the highest transdermal permeability, i.e. 1425 $\mu g/cm^2/h$. The second drug having a high permeability through skin is selegiline, used to treat major depressive disorder, which has a diffusion flux reaching 18 $\mu g/cm^2/h$. The transdermal flux of tBCEU-d_{15} after 10 hours (0.48 mg per cm^2) reported in this study (20 $\mu g/cm^2/h$) is smaller than that of nicotine, but equivalent to that of selegiline (0.3 mg per cm^2 over 24 hours) [36].

It has been shown that 100 µg of tBCEU reduced by around 50 % the tumor weight of hamster CS1 melanoma grafted onto the chick chorioallantoic membrane of developing chicks (CAM assay) [37]. Since our accumulating amount of tBCEU-d_{15} in the acceptor chamber of the Franz cell is 50 times higher than that, we believe that tBCEU-d_{15} might be a potential candidate to be used in a topical route for therapeutic applications. Other works are obviously needed to confirm such a hypothesis.

In particular, experiments should be carried out with human skin. Although different from human skin, hairless mouse skin can be considered as appropriate to test our technique platform since the present work did not have as immediate objective the demonstration that tBCEU-d15 can be successfully delivered transdermally. Mouse skin may however be used as a model to provide relevant insights into diffusion through skin [25,38]. Durrheim specifically found that within 12 hours

of diffusion experiment, the permeability of hairless mouse skin is comparable with that of human skin [39]. When such conditions are met, Heylings and co-authors showed that intact mouse skin may be an appropriate model to study subcutaneous absorption and the integrity function of skin [40,41].

However, differences between human and mouse skin do exist. Mouse skin model is different from human skin model in terms of thickness, composition, hair follicle density and permeability [42]. The thickness of human skin is about 17 μm, while that for hairless mouse skin is about 9 μm. The SC of mouse skin is richer in lipids than that of human skin. This is important since the barrier function of skin is mainly dictated by the stratum corneum, the outermost layer of epidermis. Hair follicles also play an important role in drug permeation. The hair follicle density in hairless mouse skin is nearly equal or slightly higher than that of human skin. These differences render the drugs 3-4 times more permeable in mouse skin than in human skin [43].

4.2 The influence of the experimental conditions

The results reported here are partly dictated by the conditions used in the Franz cell. In particular, they rely on the presence of organic solvents, which are supposed to improve diffusion but can cause irritation to skin. Although the potential enhancement of tBCEU permeability by solvents has not yet been investigated, its transdermal diffusion is most probably influenced by the solvent mixture chosen.

Oleic acid for example may enhance the diffusion of tBCEU-d_{15} via lipid fluidization or phase separation mechanism [44]. The presence of propylene glycol in the mixture can synergistically act with oleic acid [6,26,45] to accelerate transdermal diffusion. Ethanol is reported to permeate rapidly through skin and act as a chemical enhancer with similar effect as that of propylene glycol [45].

By contrast, the presence of DMSO in the receptor chamber may have a negligible effect on the diffusion of tBCEU-d_{15}. In order for the enhancement to be effective, the concentration of DMSO should probably be much higher. Stoughton and Cleveland indeed reported that a mixture of 40 % DMSO and 60 % ethanol was used for transport of hydrocortisone and fluocinolone through skin [46]. In the present study, only 2% DMSO was used, therefore the effect of DMSO may be small, if not insignificant.

4.3 Spatial distribution and diffusion pathway

To understand the drug distribution inside the skin, FTIR spectroscopic imaging results have been reported. Mendelsohn and co-authors studied the diffusion of solvents such as DMSO and propylene glycol on porcine skin [23]. The authors indicated that these molecules penetrate deeply into the skin up to 1-mm deep. Their results suggested that the spatial distribution of DMSO and propylene glycol is correlated with that of proteins, so that the diffusion pathway of the solvents would be related to protein-rich components of the tissue.

Our IR snapshots of skin sections suggest that the spatial distribution of tBCEU-d_{15} is not related to that of lipids. The linear correlation coefficient between lipids and tBCEU-d_{15} is almost zero (Table 1), indicating that tBCEU-d15 does not have any specific affinity for lipid-rich components in skin tissue and that its diffusion cannot be associated with a lipid-rich component. Literature data show that tBCEU can intercalate into phospholipid bilayers, causing disorder of this bilayer and lowering the phase transition temperature of the phospholipids [12]. However, it is well known that the major lipids in epidermal skin are a mixture of ceramides, fatty acids and cholesterol [47]. These molecules may not have any specific interactions with tBCEU-d_{15}, at least in the present conditions.

It may be questioned why the correlations between the amide I and amide II peak absorbance and between the $\nu_{as}(CH_2)$ and $\nu_s(CH_2)$ bands are 0.8 and 0.75, respectively, and not equal to 1 as theoretically expected. Various factors may explain this apparent discrepancy. First, there are unavoidable uncertainties/errors in the measurement of the absorbance, especially in complexes

matrices such as real skin. Second, it is possible that the absorbance of some bands may be affected by baseline variations. Finally, overlaps between the OH bending band of water and the amide I band and between the OH stretching band of water and C-H stretching band may occur. In the latter case, the overlap between the CH_2 stretching bands (mainly lipids) and the CH_3 stretching bands (mainly proteins) may complicate the signal. Despite non-zero correlation coefficients, our data could not demonstrate that a correlation exists between the spatial distribution of tBCEU and proteins. Therefore, although it cannot be excluded that the presence of tBCEU-d_{15} could be associated with skin regions where the protein concentration is low, it seems that tBCEU distribution is not related with that of proteins. In the present experiments, tBCEU is distributed at low concentration throughout mouse skin without particular preference although some high-concentrated clusters have been observed at some places. Thus, the diffusion of tBCEU does not seem to follow the standard paradigm which stipulates that the diffusion of a drug should be promoted by lipid-rich or protein-rich domains of skin. We interpret this result as an indication that tBCEU-d_{15} diffuses across skin through solution-diffusion mechanism, which has been used to explain the permeability of substances through reverse osmosis membrane. Thus, the molecules apparently do not need to have any specific affinity with the components of skin.

Table I. Correlation coefficients (with their standard deviations) between the spatial intensity variations of bands due to tBCEU-d15, lipids and proteins.

Intensity variables X/Y	Pearson correlation coefficient[1]	Standard deviation
amide I/amide II	0.801	0.060
$\nu_{as}(CH_2)/\nu_s(CH_2)$	0.752	0.140
$\nu_{as}(CD_3)$/amide II	-0.361	0.010
$\nu_{as}(CD_3)$/amide I	-0.416	0.010
$\nu_{as}(CD_3)/\nu_{as}(CH_2)$	0.048	0.015
$\nu_{as}(CD_3)/\nu_s(CH_2)$	-0.151	0.021

[1] Intensities were measured on 50 pixels where the absorption intensity of $\nu_{as}(CD_3)$ is the highest. Correlation coefficients were calculated from the average of five different mouse skin slices.

If the membrane was homogeneous in term of composition, the concentration of tBCEU-d_{15} should be gradually reduced from the donor chamber–skin interface to skin–acceptor chamber one. Yet, the skin is not perfectly homogeneous as it is composed of several layers (epidermis, dermis and hypodermis) and has a varying transverse chemical composition and anatomical structure. Laterally, the skin varies both in thickness and composition [48-50]. This natural heterogeneity is responsible for the discontinuous nature of skin and may cause interruption in transport of drug molecules [51]. Besides, reservoir exist in some locations within skin [52]. This can help explaining why tBCEU-d_{15} accumulates in some regions, as evidenced by IR images. In addition, if the purpose is to transport tBCEU through skin and enter the circulation system, then the fact that this molecule does not have any specific attachment with skin is a positive property. However, if the purpose is to deliver tBCEU to a target, then the molecules should have some kinds of specific affinity, whether

with the normal tissue components or with tumor cell. To this aim, tBCEU molecules may be functionalized or encapsulated inside a specific carrier, which has selective attachment with normal tissues. Alternately, encapsulation may be an option. In addition, the membrane of tumor cells may expose some particular kind of functional groups that may display a specific attachment with tBCEU.

4.4 The influence of the physical state of tBCEU

It is particularly interesting to note that tBCEU is in a crystalline form in skin. Rationalizing the whole data set, it may be inferred that tBCEU is relatively rapidly conveyed throughout skin by the solvent mixture with no (visible) preferential pathway. The propensity of tBCEU to crystallize may promote the formation of nuclei and crystal domains, especially as the solvent progresses and evaporates. The crystallization of drugs in skin is not new and has already been observed [52]. Raman spectroscopy has been successfully used to identify polymorphic forms of substances in Pharmacopoeias, both in vitro and in vivo [52,53]. Although IR spectroscopy has been used for polymorph differentiation of a variety of substances [54], to our knowledge it has not been applied for the detection of crystal substances in skin. Burgina and coworkers used IR spectroscopy to distinguish paracetamol and phenacetin in solution and in crystalline state [55].

It is worth noting that the crystallization of drugs inside the skin may pose a challenge for transdermal delivery. The ideal drug should dissolve in body fluids and enter the circulation system for treatment effectiveness so that drug accumulation in some regions of the skin may be considered as reservoirs. It has been suggested that the crystallization of active drugs may be exploited for control release [52]. Otherwise, another way to overcome the crystallization of tBCEU-d15 inside the skin is to encapsulate it inside a nano-carrier for delivery.

5 CONCLUSIONS

This study is, to our knowledge, the first report on the imaging of spatial distribution of small-drug molecules across full-thickness skin, confirmed by Franz cell experiments and FTIR spectroscopic imaging characterization. It shows that tBCEU-d15 penetrates and diffuses across hairless mouse skin. No preferential transdermal pathway has been evidenced. The penetration properties of tBCEU then make it a potential candidate for transdermal therapy, but more work is needed to confirm this hypothesis. The present study also emphasizes the powerful advantages of FTIR imaging for transdermal absorption investigation, showing that the spatial distribution of tBCEU-d_{15} inside the skin is not correlated with that of lipids or proteins and allowing inference of the physical state of tBCEU.

ACKNOWLEDGEMENTS

The authors thank Andrée-Anne Guay-Bégin, Pascale Chevallier, Stéphanie Fournier and François Paquet-Mercier for their invaluable technical support. This work was supported by the Fonds de Recherche du Québec-Nature et technologies (FRQNT) and the Natural Sciences and Engineering Research Council (NSERC) of Canada. The Regroupement québécois de recherche sur la fonction, l'ingénierie et les applications des protéines (PROTEO), the Centre de recherche sur les matériaux avancés (CERMA) and the Centre québécois sur les matériaux fonctionnels (CQMF) are also acknowledged for providing their instrumental infrastructure. The authors state no conflict of interest.

REFERENCES

[1] M. R. Prausnitz, S. Mitragotri, R. Langer, Current status and future potential of transdermal drug delivery. Nat. Rev. Drug Discov. 3 (2004), 115-124.

[2] M. R. Prausnitz, R. Langer, Transdermal drug delivery. Nat. Biotechnol. 26 (2008), 1261-1268.
[3] C. M. Schoellhammer, D. Blankschtein, R. Langer, Skin permeabilization for transdermal drug delivery: Recent advances and future prospects. Expert Opin. Drug Del. 11 (2014), 393-407.
[4] S. Wiedersberg, R. H. Guy, Transdermal drug delivery: 30+ years of war and still fighting! J. Control. Release 190 (2014), 150-156.
[5] F. Bassyouni, N. ElHalwany, M. Abdel Rehim, M. Neyfeh, Advances and new technologies applied in controlled drug delivery system. Res. Chem. Intermed. 41 (2013), 2165-2200.
[6] M. E. Lane, Skin penetration enhancers. Int. J. Pharm. 447 (2013), 12-21.
[7] R. C.-Gaudreault, J. Lacroix, M. Pagé, L. P. Joly, 1-aryl-3-(2-chloroethyl) ureas: Synthesis and in vitro assay as potential anticancer agents. J. Pharm. Sci. 77 (1988), 185-187.
[8] A. Saint-Laurent, N. Boudreau, R. C.-Gaudreault, P. Poyet, M. Auger, Interaction between lipid bilayers and a new class of antineoplastic agents derived from arylchloroethylurea: A 2H solid-state NMR study. Biochem. Cell Biol. 76 (1998), 465-471.
[9] E. Miot-Noirault et al., Antineoplastic potency of acrylchloroethylurea derivatives in murine colon carcinoma. Invest. New Drug 22 (2004), 369-378.
[10] E. Mounetou, E. Miot-Noirault, R. C.-Gaudreault, J. C. Madelmont, N-4-iodophenyl-N'-2-chloroethylurea, a novel potential anticancer agent with colon-specific accumulation: radioiodination and comparative in vivo biodistribution profiles. Invest. New Drug 28 (2009), 124-131.
[11] A. Patenaude et al., Chloroethyl urea derivatives block tumour growth and thioredoxin-1 nuclear translocation. Can. J. Physiol. Pharmacol. 88 (2010), 1102-1114.
[12] C. Gicquaud et al., Interaction of 4-tert-butyl-[3-(2-chloroethyl) ureido]benzene with phosphatidylcholine bilayers: A differential scanning calorimetry and infrared spectroscopy study. Arch. Biochem. Biophys. 334 (1996), 193-199.
[13] A. Saint-Laurent et al., Membrane interactions of a new class of anticancer agents derived from arylchloroethylurea: A FTIR spectroscopic study. Chem. Phys. Lipids 111 (2001), 163-175.
[14] L. Bartosova, J. Bajgar, Transdermal drug delivery in vitro using diffusion cells. Curr. Med. Chem. 19 (2012), 4671-4677.
[15] R. Mendelsohn, M. E. Rerek, D. J. Moore, Infrared spectroscopy and microscopic imaging of stratum corneum models and skin. Phys. Chem. Chem. Phys. 2 (2000), 4651-4657.
[16] M. Leroy, T. Lefèvre, R. Pouliot, M. Auger, G. Laroche, Using infrared and Raman microspectroscopies to compare ex vivo involved psoriatic skin with normal human skin. J. Biomed. Opt. 20 (2015), 067004.
[17] M. Leroy, M. Lafleur, M. Auger, G. Laroche, R. Pouliot, Characterization of the structure of human skin substitutes by infrared microspectroscopy. Anal. Bioanal. Chem. 405 (2013), 8709-8718.
[18] M. Leroy et al., A comparative study between human skin substitutes and normal human skin using Raman microspectroscopy. Acta Biomater. 10 (2014), 2703-2711.
[19] C. Xiao, D. J. Moore, M. E. Rerek, C. R. Flach, R. Mendelsohn, Feasibility of tracking phospholipid permeation into skin using infrared and raman microscopic imaging. J. Invest. Dermatol. 124 (2005), 622-632.
[20] Q. Zhang et al., Infrared spectroscopic imaging tracks lateral distribution in human stratum corneum. Pharm. Res. 31 (2014), 2762-2773.
[21] B. W. Barry, H. G. M. Edwards, A. C. Williams, Fourier Transform Raman and infrared vibrational study of human skin: Assignment of spectral bands. J. Raman Spectrosc. 23 (1992), 641-645.
[22] P. Garidel, Insights in the biochemical composition of skin as investigated by micro infrared spectroscopic imaging. Phys. Chem. Chem. Phys. 5 (2003), 2673-2679.
[23] R. Mendelsohn, H. C. Chen, M. E. Rerek, D. J. Moore, Infrared microspectroscopic imaging maps the spatial distribution of exogenous molecules in skin. J. Biomed. Opt. 8 (2003), 185-190.
[24] P. Béchard, J. Lacroix, P. Poyet, R. C.-Gaudreault, Synthesis and cytotoxic activity of new alkyl[3-(2-chloroethyl)ureido]benzene derivatives. Eur. J. Med. Chem. 29 (1994), 963-966.

[25] T. Kai, V. H. W. Mak, R. O. Potts, R. H. Guy, Mechanism of percutaneous penetration enhancement: effect of n-alkanols on the permeability barrier of hairless mouse skin. J. Control. Release 12 (1990), 103-112.
[26] B. W. Barry, Mode of action of penetration enhancers in human skin. J. Control. Release 6 (1987), 85-97.
[27] P. D. A. Pudney, M. Melot, P. J. Caspers, A. van der Pol, G. J. Puppels, An in vivo confocal Raman study of the delivery of trans-retinol to the skin. Appl. Spectrosc. 61 (2007), 804-811.
[28] F. Biagini, M. Campanino, Elements of probability and statistics. (2015) vol. 98, pp. 23-25.
[29] J. L. Rodgers, W. A. Nicewander, Thirteen ways to look at the correlation coefficient. Am. Stat. 42 (1988), 59-66.
[30] P. Garidel, Structural organisation and phase behaviour of a stratum corneum lipid analogue: ceramide 3A. Phys. Chem. Chem. Phys. 8 (2006), 2265-2275.
[31] S. Krimm, J. Bandekar, Vibrational spectroscopy and conformation of peptides, polypeptides, and proteins. Adv. Protein Chem. 38 (1986), 181-364.
[32] B. Nolin, R. N. Jones, The infrared absorption spectra of diethyl ketone and its deuterium substitution products. J. Am. Chem. Soc. 75 (1953), 5626-5628.
[33] T. Schafer, A. Kandratsenka, P. Vohringer, J. Schroeder, D. Schwarzer, Vibrational energy relaxation of the ND-stretching vibration of NH2D in liquid NH3. Phys. Chem. Chem. Phys. 14 (2012), 11651-11656.
[34] J. Pliva, J. W. C. Johns, L. Goodman, High-resolution study of the C-D stretching bands of 12C6D6 and 13C6D6. J. Mol. Spectrosc. 163 (1994), 108-118.
[35] M. Flak, E. Whalley, Infrared spectra of methanol and deuterated methanols in gas, liquid, and solid phases. J. Chem. Phys. 34 (1961), 1554-1568.
[36] Emsam® (segeline transdermal system) - Continuous delivery for once-daily application (2007), https://www.accessdata.fda.gov/drugsatfda_docs/nda/2006/021336s000_021708s000TOC.cfm, accessed: 2nd october 2017).
[37] T. Petitclerc et al., Antiangiogenic and antitumoral activity of phenyl-3-(2-chloroethyl)ureas: A class of soft alkylating agents disrupting microtubules that are unaffected by cell adhesion-mediated drug resistance. Cancer Research 64 (2004), 4654-4663.
[38] H. Durrheim, G. L. Flynn, W. I. Higuchi, C. R. Behl, Permeation of hairless mouse skin I: Experimental methods and comparison with human epidermal permeation by alkanols. J. Pharm. Sci. 69 (1980), 781-788.
[39] J. R. Bond, B. W. Barry, Limitations of hairless mouse skin as a model for in vitro permeation studies through human skin: Hydration damage. J. Invest. Dermatol. 90 (1988), 486-489.
[40] J. R. Heylings et al., Sensitization to 2,4-dinitrochlorobenzene: Influence of vehicle on absorption and lymph node activation. Toxicology 109 (1996), 57-65.
[41] J. R. Heylings, H. M. Clowes, L. Hughes, Comparison of tissue source for the skin integrity function test (SIFT). Toxicol. in Vitro 15 (2001), 597-600.
[42] H. Todo, Transdermal permeation of drugs in various animal species. Pharmaceutics 9 (2017), 33.
[43] B. Ghosh, H. Reddy, R. V. Kulkarni, J. Khanam, Comparison of skin permeability of drugs in mice and human cadaver skin. Indian J. Exp. Biol. 38 (2000), 42-45.
[44] A. Naik, L. A. R. M. Pechtold, R. O. Potts, R. H. Guy, Mechanism of oleic acid-induced skin penetration enhancement in vivo in humans. J. Control. Release 37 (1995), 299-306.
[45] A. C. Williams, B. W. Barry, Penetration enhancers. Adv. Drug Deliver. Rev. 56 (2004), 603-618.
[46] R. B. Stoughton, Dimethylsulfoxide (DMSO) - Induction of a steroid reservoir in human skin. Arch. Dermatol. 91 (1965), 657-660.
[47] A. Pappas, Epidermal surface lipids. Dermatoendocrinol. 1 (2009), 72-76.

[48] N. V. Alexeeva, M. A. Arnold, Near-infrared microspectroscopic analysis of rat skin tissue heterogeneity in relation to noninvasive glucose sensing. J. Diabetes Sci. Technol. 3 (2009), 219-232.
[49] N. V. Alexeeva, M. A. Arnold, Impact of tissue heterogeneity on noninvasive near-infrared glucose measurements in interstitial fluid of rat skin. J. Diabetes Sci. Technol. 4 (2010), 1041-1054.
[50] R. R. Driskell, F. M. Watt, Understanding fibroblast heterogeneity in the skin. Trends Cell Biol. 25 (2014), 92-99.
[51] M. M. Q. Xing, N. Pan, W. Zhong, X. Hui, H. I. Maibach, Interfacial kinetics effects on transdermal drug delivery: a computer modeling. Skin Res. Technol. 14 (2008), 165–172.
[52] J. Hadgraft, M. E. Lane, Drug crystallization – implications for topical and transdermal delivery. Expert Opin. Drug Del. 13 (2016), 817–830.
[53] M. E. Auer, U. J. Griesser, J. Sawatzki, Qualitative and quantitative study of polymorphic forms in drug formulations by near infrared FT-Raman spectroscopy. J. Mol. Struct. 661-662 (2003), 307-317.
[54] D. N. Kendall, Identification of polymorphic forms of crystals by infrared spectroscopy. Anal. Chem. 25 (1953), 382-389.
[55] E. B. Burgina, V. P. Baltakhinov, E. V. Boldyreva, T. P. Shakhtschneider, IR spectra of paracetamol and phenacetin. 1. Theoretical and experimental studies. J. Struct. Chem 45 (2004), 64-73.